Solid Freeform Fabrication 2023: Proceedings of the 34th Annual International Solid Freeform Fabrication Symposium – An Additive Manufacturing Conference
Reviewed Paper

RESIDUAL STRESS AND DEFORMATION ANALYSIS OF INCONEL 718 ACROSS VARYING OVERHANGS IN LASER POWDER BLOWN DIRECTED ENERGY DEPOSITION

A. J. Hernandez[1*], D. Garcia[1], K. I. Watanabe[1], P. R. Gradl[2], K. Wheeler[3], Halyna Hafiychuk[4], R. B. Wicker[1], F. Medina[1]

[1] W.M. Keck Center for 3D Innovation, El Paso, TX, 79902, USA

[2]NASA, Marshall Space Flight Center, Huntsville, Al, 35812, USA

[3] NASA, Ames Research Center, Moffett Field, CA, 94035, USA

[4] KBR Wyle Services, Ames Research Center, Moffett Field, CA, 94035, USA

* Corresponding author (Ajhernandez24@miners.utep.edu)

Keywords: *DED, residual stress, deformation, overhangs, simulation*

Abstract

Any metal that is subjected to rapid heat and cooling will undergo the development of residual stresses. As they experience intense temperature fluctuations, this will consequently alter the way the material will behave. This issue proves to be of great concern within additive manufacturing. That said, the presence of temperature fluctuations is more prominent in Directed energy deposition (DED), whereas other methods of manufacturing are more prominent in the pre- or post- printing process. This in turn means the deformation, as well as the redistribution of the residual stresses within pieces, are subject to variance by several process parameters set during a print. By using the Inconel 718 alloy feedstock in RPMI's Laser Powder Directed Energy Deposition (LP-DED) printer, a series of coupons with four different overhang angles and laser power outputs will determine how these changes thermo-mechanically affect the prints through the use of FEA simulations and scans.

Introduction

Directed Energy Deposition (DED) has been increasingly utilized for over the past 3 decades and is known for fabricating high strength and durable products [1]. Its services primarily come into use with applications such as cladding and repair work. These services are useful and are becoming increasingly utilized by those within the aerospace, automotive and other industries who work with similar heavy machinery [1]. Directed Energy Deposition has a wide assortment of processes in how they print their feedstock, and this work focuses on the use of a laser powder feedstock-based system. Sandia National Laboratories originally developed the

method of a powder fed laser printing system using what is known as Laser Engineered Net Shaping (LENS), which later inspired other variants of such process from companies such as TRUMPF Inc., RPM Innovations, and EFESTO Inc. [2].

The general process proceeds as follows: metal powder feedstock is fed onto the build area using a pneumatic system, where the feedstock is blown out through a nozzle that forms a cross fed region onto a build substate. This region is then melted onto the build substrate and subsequently built on top of previously deposited material to create layers using an optical system that concentrates a laser onto the area. The nozzle and laser are manned by a gantry that is programmed to follow a toolpath set by the user [2] by commands using programming languages such as G-code [2].

The absence of a powder bed and increased laser power output relative to that of laser powder bed fusion comes with its own obstacles. Thermal gradients and rapid cooling rates that result from this method of printing lead to undesired residual stress that develops within the component being built. This results in reduced mechanical performance such as applied load-related fractures and shortened service life of components[2]. The components can go through heat treatments and machine finishes to alleviate the stress, but that does not expand on the full capabilities of DED can have that could help mitigate the residual stress issue [2]. It is a point of interest as to what other variables can impact the stress distribution throughout the body. Especially if such variables like residual stress or geometric factors such as deformation and overhang angles can be observed through FEA. Such correlations can aid in targeting limitations and improved printing strategies for future builds.

Literature Review

Previous works have shown that higher laser power output with a lower laser velocity led to negative impacts to the structure such as keyhole pores, cracks, and uneven deposition [3]. The inverse negates most of these defects but with the increased probability of lack of fusion occurring. This will reflect onto the mechanical testing as either of these defects can reduce the Ultimate Tensile Strength (UTS) and the fatigue life cycle. There have also been reports where the top sections of the build tend to perform poorer than the bottom sections with tests such as tensile testing due to variance in microstructure within the build [4]. There has not been enough evidence to indicate that the stress distribution within the build is a major factor in this difference in performance. However, it would be of interest if the overhang angles have any influence on this trend.

What has been noted about the residual stress development while using Inconel 718 is that said material tends to augment differently based off the substrate used. This is due to the recrystallization process that causes irregular grain patterns and in turn creates an accumulation of stress [5] near the bases of all coupons. The as built conditions typically depict columnar dendritic microstructures [5] that lead to reduced performance than if they were heat treated. The long linear composition promotes the propagation of cracks.

Thermal fluctuations are of concern as well when working with metals since their effect can come from external sources such as the substrate to the main feedstock. An unprepared substrate can potentially distort the initial layers of deposition due to the increased Maximum Thermal Gradients (MTG) the material experiences as compared to later stages in the build [6]. Substrate size is also a factor of importance as a thicker substrate generally reduces thermal deformation, but a more rigid substrate suscepts the build to experience more plastic deformation as it cools down [6].

Methods

The printer used for the experiment is RPMI's 222XR model. It is a Laser Powder Directed Energy Deposition (LP-DED). The laser installed can output up to 2000 W using an IPG Fiber Laser. The 222XR model possesses the ability to build free standing overhangs of up to 35 degrees. As for the chamber, the printer performs under an argon rich atmosphere and contains external powder hoppers that minimize the oxidation that occurs while printing.

The project consists of using virgin Inconel 718 of around 45-150 microns to produce 8 prints with varying slants implemented onto the side walls. These variants include slant boxes, otherwise known as coupons, with an overhang angle of either 0 º, 20 º, 30 º, or 35 º(Figure 1). The parameters of the coupons were modified to accommodate the laser power output to properly print the coupons. Such parameters are layer thickness, widths, spot size, hatch width, powder flow rate, and printing speeds for the two lasers outputs of 1070 and 2000 W (Table 1). These parameters were to reduce the appearance of defects such as over deposition, keyholing, and lack of fusion. The coupons were all printed in an argon environment with less than 10 ppm of oxygen.

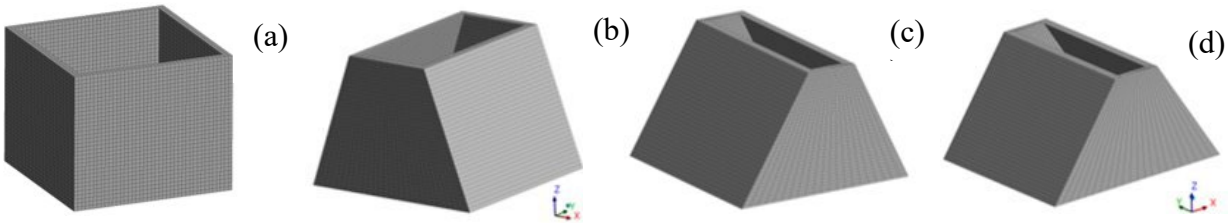

Figure 1: CAD models of 0º (a), 20º (b) ,30º (c), 35º (d) slant-walled coupons

RPMI 222XR Coupon Parameters								
Laser Power	End part thickness	STL Thickness	Spot size	Hatch Width	Layer Thickness	Powder Flow Rate	Contour Speed	Hatch Speed
1070 W	.250”	.180”	.070”	.045”	.015”	11 g/min	32 IPM	40 IPM
2000 W	.325”	.220”	.105”	.070”	.025”	13 g/min	28 IPM	40 IPM

Table 1: Parameters of coupons built based off laser power

Coupon thickness varied in with the lower measurements starting at 4.57 all the way up to 10.16 mm as we increased the overhang angle and laser output of the coupons. This was a preventative measure to reduce the risk of overheating the Inconel 718 if not properly adjusted for such wattage. The scanning pattern used was an arbitrary hatch pattern with an internal and external contour to print the layer. Each layer completed was followed by a dwell time of 10 seconds to allow for component cooling. The hatching directions, although meant to fill any voids that can affect mechanical properties, are also a potential factor in shift in stress distribution and in turn performance [7]. For the intent of this experiment, scanning strategies will not be comparable due to several modifications primarily based on laser power and overhang angles.

It is generally of common knowledge that the worst mechanical behavior of a component is generally in the direction that it is being built, even in metal printing [7]. It is possible that the directional stress accumulation is most intense in these directions as well. This leads to the assumption that the stress in the other directions facilitates a poorer performance of the coupons. The material shrinkage that occurs when Inconel 718 is left to cool after being deposition and fusion is the reason that the other directional stresses must be accounted for [7].

As stated before, the RPMI 222XR model is capable of reproducing builds without the need for supports. In fact, the lack of support helps retain the as built build superficial integrity of a build [8]. support orientation is also a factor that can ultimately alter the mechanical performance of the final product, hence it was of best interest to avoid the implementation of any supports where possible [8]. free formed overhang angle capabilities will vary based on the printer’s gantry and modification of orientation mid-build and should specified in any modelling process to preserve accuracy.

To maintain consistency, Stainless steel build plates with a thickness of ½" and ¾” or more were used for the 1070 W and 2000 W prints respectively. Each plate was cut with an approximate 6”x6” length, with clamps placed on each of the corners to reduce plate warping. This in turn leads to an overall reduced external stress and deformation imposed on the coupon. The build plates surfaces were machined to remove any finishes and tarnishes it had to gain better fusion. Another point to note is that after initial residual stress analysis of the coupons still attached to the substrates, the coupons were sectioned off the build plate and underwent another

analysis to track any additional deformation and stress shift that can occur as to promote a 'final' residual stress state [4]. The gantry had a 4-powder coaxial feed nozzle with the nozzles having 45º tilt and 23º tilt respective to the power source for the 1070-W and 2000-W respectively (Figure 2). This design would benefit a high catchment rate, as similar experiments using a coaxial feed nozzle had recorded high a powder catchment efficiency of up to 80% and has a uniform feed rate across nozzles that translate to a uniformly shaped melt bead [9].

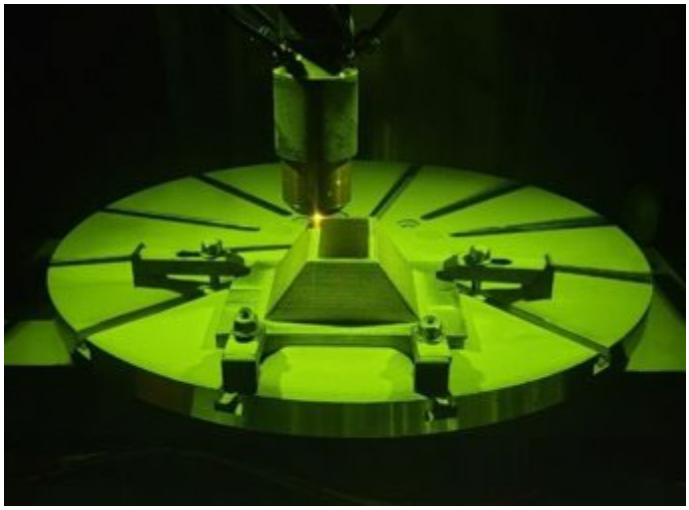

Figure 2: Slant box (coupon) in build set-up

FEA Modelling

Typically, to remain as accurate to the build, simulation software can incorporate vital parameters to mimic to the actual build such as laser output, deposition height, scan path, and dwell time [10]. Mesh size and shape for the coupons are also a significant factor in the accuracy of the results we obtain, but in turn increase the amount of processing power and time needed to compute a simulation. For that reason, a compromise is made where an acceptable accuracy error percentage still constitutes a viable simulation based on clientele preference. One such element shape that can provide accurate results is the hexahedron element. As the coupons being analyzed are simplistic in shape and design, the hexahedron element provides a high capability in preserving features such as edges, curves, and overhangs. This will serve beneficial in simulations such as distortion where a lower resolution mesh such as one with tetrahedron elements cannot capture small scale warping in units such as the hundred microns range. One other way is to capture a thermo-mechanical simulations one way coupling, that allows for one variable to become time dependent while the others remain static (i.e., the thermal history can be time dependent, whereas the structural mechanics of a build remains a static study). Some software is able capable of reproducing the laser up to its size, shape, and efficiency [12] in their computations.

For the coupon simulations, the ANSYS Additive Workbench with a Directed Energy Deposition add-on package was utilized to compute the results. Such material characteristic

curves as a function of temperature used within the ANSYS parameters available include specific heat, thermal conductivity, density as well as structural parameters Young's Modulus, Poisson ratio, coefficient of thermal expansion, Yield stress, and a Hardening curve parameter. Additional conditions that were put in place were a convective boundary condition of 10 W/m^2, distortion compensation factors, and the filleting of the coupon CAD's edges similar to that of the laser light measurements done on the coupons (Figure 3). This fillet action is done in to replicate the definition of the corners and edges of the actual coupons when in simulation. Coupons were simulated both on and sectioned off the substrate. Other factors that are considered were the process parameters used for manufacturing in-situ. The geometries of the coupons were converted in a mesh with two cartesian cells orthogonal to the wall and adapted by using a 250 mm^3 cluster model and modified with the previously mentioned fillet for all further simulations (Figure 4,5).

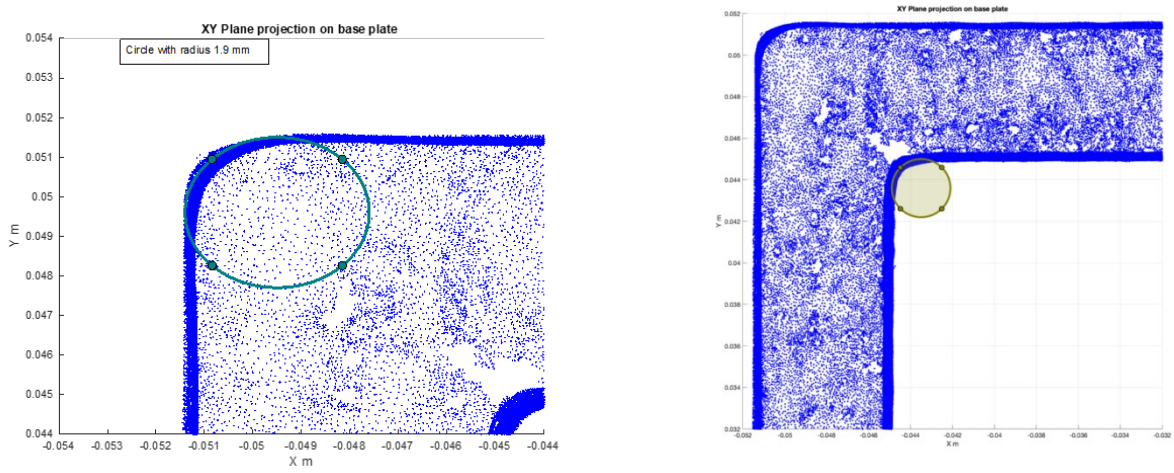

Figure 3: Examples of radii measurements of 1070-Watt vertical wall using laser light scanner for fillet

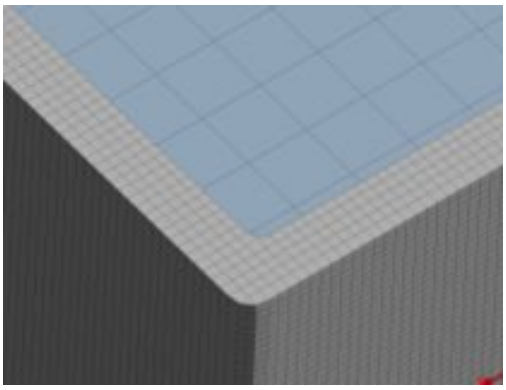

Figure 4: Close up of filleted edge on 0-degree wall mesh

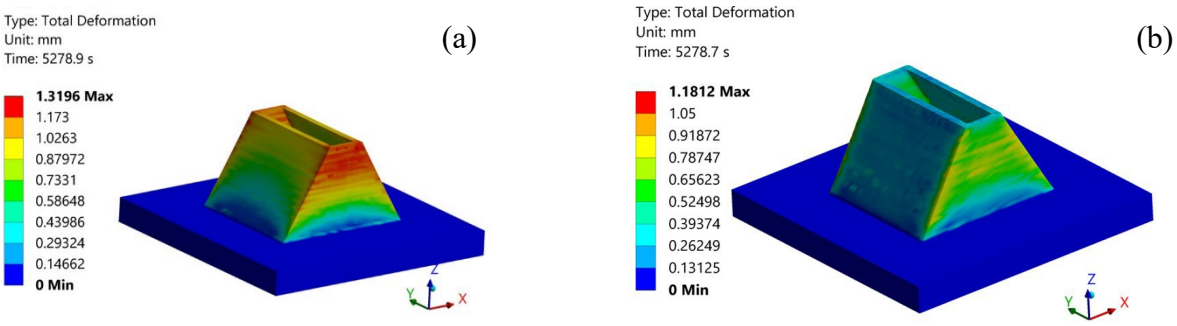

Figure 5: Difference of results with (a) and without (b) fillet using total deformation simulation

Results

From the simulations input parameters, residual stresses were computed in the x, y, and z direction. Directional deformation simulations were also performed and cross-referenced between select models that were analyzed using an ATOS 5 structured light scanner to compose the 3D models. Other simulations and scans that were conducted include sectioned coupons from the substrate and the coupon measurement of the radii.

The residual stresses were obtained for all boxes and two laser powers. Using the 20 º wall at 1070-W coupon (Figure 6) as reference, most of the coupons in both laser powers exhibit the same stress patterns in their respective directional simulation regardless of the angle deviation that was implemented. The stress appears to concentrate at the edges of the coupons as well as the regions where the feedstock is closest to the substrate. The results below depict that there is no definitive correlation between increasing the angle of the slant wall and the shift of the stresses that accumulate, the 30 º slant wall had the more intense stresses throughout most the simulations (Table 2). These stresses were most prominent parallel to the edges parallel to what ever direction the stress simulations were done in.

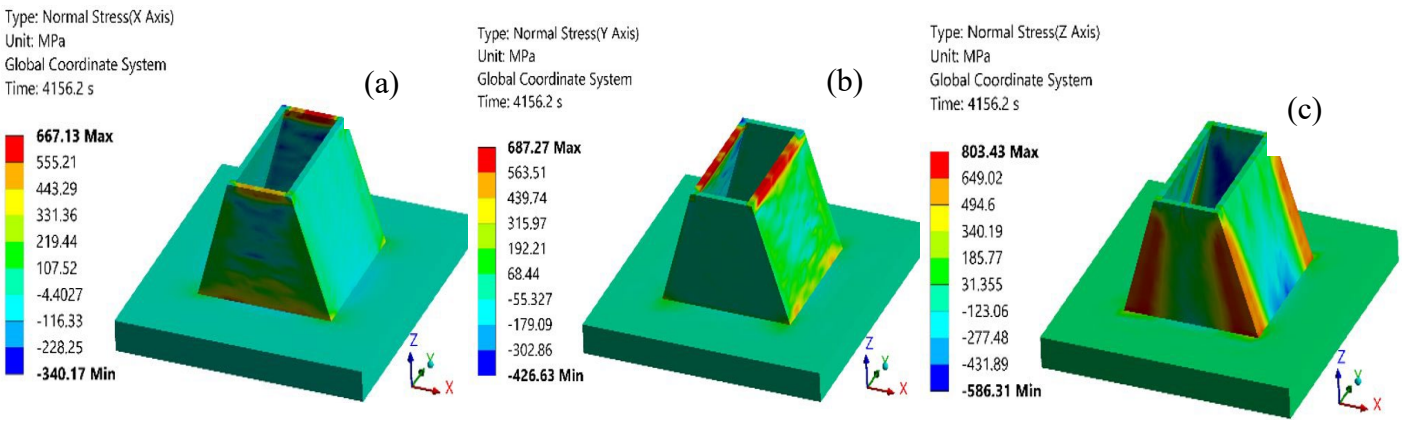

Figure 6: Directional residual stress analysis of 20° wall at 1070 W in X (a), Y (b), and Z (c) direction

Directional Residual Stress Accumulation in 1070 Watt Coupons (MPa)- Unsectioned						
Degree	X axis		Y axis		Z axis	
	Tensile	Compressive	Tensile	Compressive	Tensile	Compressive
0	695.68	563.12	691.92	525.11	857.99	531.07
20	667.13	340.17	687.27	426.63	803.43	586.31
30	797.39	559.44	810.19	685.98	807.58	801.57
35	711.15	465.61	845.91	450.1	854.58	662.23

Table 2: Directional Residual Stress Accumulation in 1070-Watt Coupons (MPa)- Unsectioned

Sectioned off coupons in the simulation presented a considerable stress pattern change than their initial simulations with the substrate still attached to them. The most prominent change is the alleviation of stress at the bottom corners of the coupons in the z-axis. The x and y-axis, however, now shifted the stress and concentrated it in the bottom middle sections of the wall where they were sectioned off from. The simulated data also suggests that the 30 º slant wall develops the most stress just like the unsectioned FEA set, except for the stresses in the z-axis being most intense in the 45 º slant wall (Table 3).

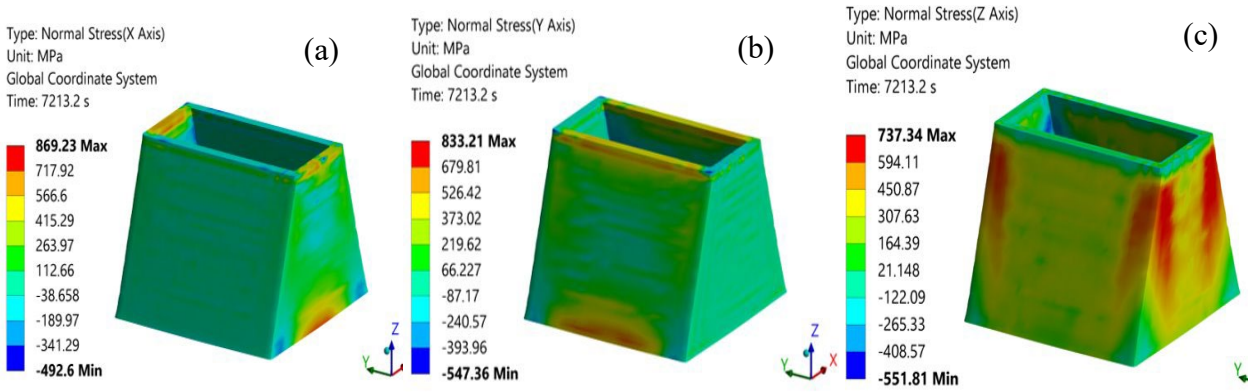

Figure 7: Directional residual stress analysis of 20° wall sectioned off substrate at 2000 W in x (a), y (b), and z (c) direction

Directional Residual Stress Accumulation in 2000-Watt Coupons (MPa) - Section						
Degree	X axis		Y axis		Z axis	
	Tensile	Compressive	Tensile	Compressive	Tensile	Compressive
0	847.45	563.12	842.73	566.98	727.76	592.50
20	869.23	492.6	833.21	547.36	737.34	551.81
30	970.43	649.55	846.79	799.50	890.97	590.77
35	800.42	491.41	757.62	618.08	930.57	647.55

Table 3: Directional Residual Stress Accumulation in 2000-Watt Coupons (MPa)- sectioned

The deformation simulation (Figure 8,9) computed results of a pattern close to that of the actual measurements retrieved from the ATOS 5 (Figure 10,11). The deformation appeared to mimic a similar pattern to that of the stress distribution of the sectioned coupon simulation seen previously. The maximum distortion recorded only went up to about .004 in, a minute measurement in retrospect to the size of the coupon, but in turn demonstrating low distortion action while in its as-built condition.

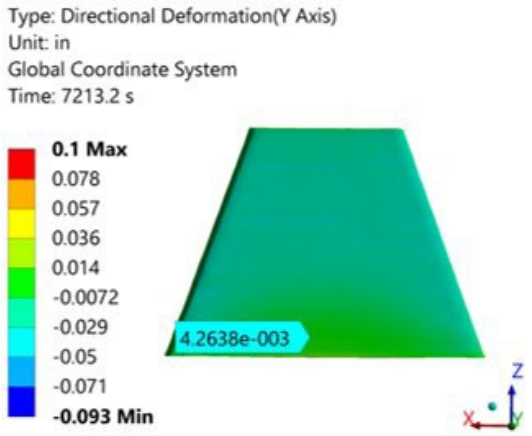

Figure 8: Y-axis Directional deformation of 20° wall at 2000 W in the Y-axis

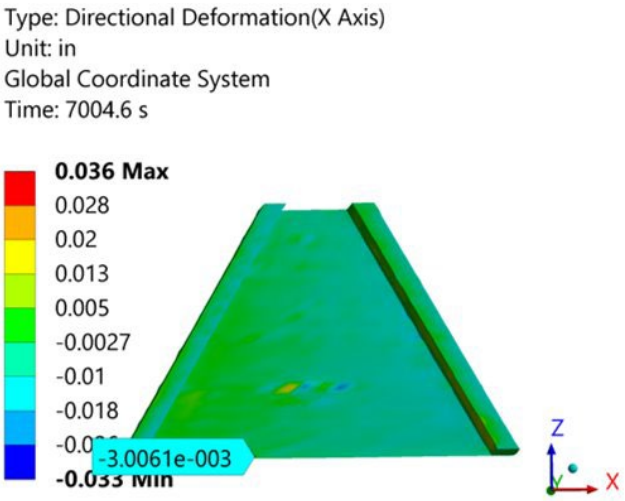

Figure 9: X-axis Directional deformation of 20° wall at 2000 W in the x-axis

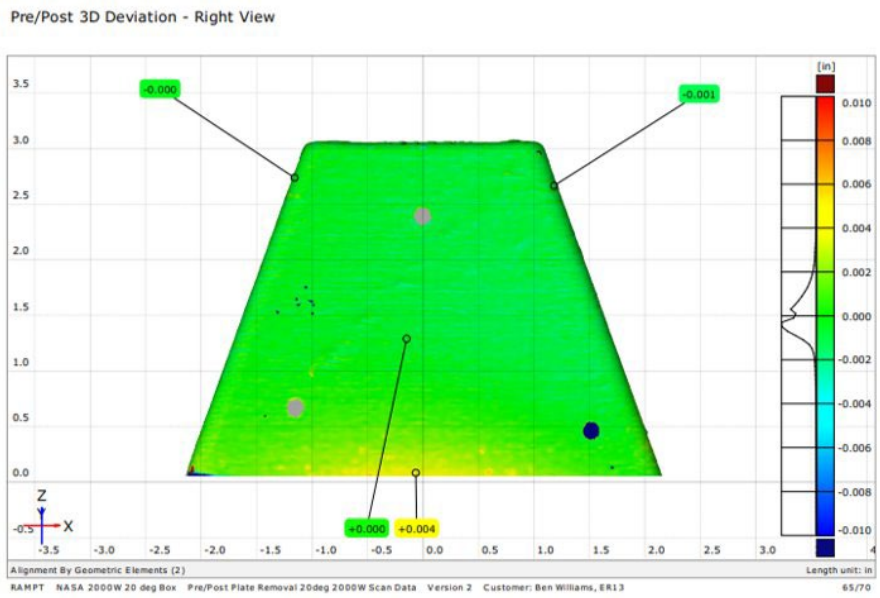

Figure 10: Laser light scanned deformation of 20º wall at 2000 W in the y-axis

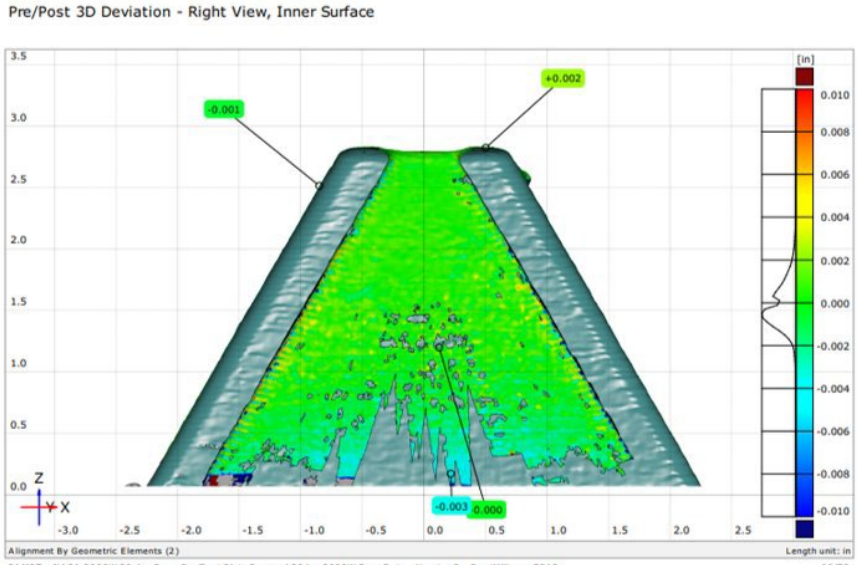

Figure 11: Laser light scanned deformation of 20º wall at 2000 W in the x-axis

Conclusion

From what we have gathered so far, the 30 º slant wall angle seems to be the most detrimental in terms of accumulating the most stress. The stresses themselves do not have a

definitive correlation as the slant wall angle increases. The experiment also indicates that other geometric features such as corners and edges as well as external forces such as thermal history and substrates within the experiment have a greater magnitude of influence on the build's residual stress profile. Structured light scans suggest that deformation occurs most prominently wherever the most tensile stress is present, albeit whenever external stimuli such as sectioning affects said area.

The project still has intentions on doing a neutron diffraction analysis on the boxes to visualize the material's structures in its as built state before initiating endeavors such as heat treatments and destructive testing. Possible testing includes doing either tensile testing from different sections of the wall or fatigue testing using the same sections. This will be dependent on the types of specimens we can derive from the piece. Hence, specimen design will require a lot of focus due the variance in wall thickness between coupons. It is also of interest to conduct metallography to determine any unforeseen defects that will aid how each coupon should perform mechanically.

Acknowledgements

Contributions and acknowledgements to the simulation and light scan work conducted include Kevin Wheeler, Halyna Hafiychuk, and others associates from NASA. The in-situ work was performed with staff member Kurtis Watanabe alongside with graduate students Alejandro Hernandez and Dajalma Garcia under the mentorship of Francisco Medina at the W.M. Keck Center for 3D Innovation at the University of Texas at El Paso, El Paso, TX, 79968 USA.

References

[1] Svetlizky, D., Das, M., Zheng, B., Vyatskikh, A. L., Bose, S., Bandyopadhyay, A., Schoenung, J. M., Lavernia, E. J., & Eliaz, N. (2021). Directed energy deposition (DED) additive manufacturing: Physical characteristics, defects, challenges, and applications. *Materials Today*, *49*, 271–295.

[2] Ahn, D.-G. (2021). Directed energy deposition (DED) process: State of the art. *International Journal of Precision Engineering and Manufacturing-Green Technology*, *8*(2), 703–742.

[3] Mazzucato, F., Forni, D., Valente, A., & Cadoni, E. (2021a). Laser metal deposition of Inconel 718 alloy and as-built mechanical properties compared to casting. *Materials*, *14*(2), 437.

[4] Li, Z., Chen, J., Sui, S., Zhong, C., Lu, X., & Lin, X. (2020). The microstructure evolution and tensile properties of Inconel 718 fabricated by high-deposition-rate laser directed energy deposition. *Additive Manufacturing*, *31*, 100941.

[5] Ramiro, P., Galarraga, H., Pérez-Checa, A., Ortiz, M., Alberdi, A., Bhujangrao, T., Morales, E., & Ukar, E. (2022). Effect of heat treatment on the microstructure and hardness of ni-based alloy 718 in a variable thickness geometry deposited by powder fed directed energy deposition. *Metals*, *12*(6), 952.

[6] Lu, X., Chiumenti, M., Cervera, M., Li, J., Lin, X., Ma, L., Zhang, G., & Liang, E. (2021). Substrate design to minimize residual stresses in directed energy deposition AM processes. *Materials & Design*, *202*, 109525.

[7] Weisz-Patrault, D., Margerit, P., & Constantinescu, A. (2022). Residual stresses in thin walled-structures manufactured by directed energy deposition: In-situ measurements, fast thermo-mechanical simulation and buckling. *Additive Manufacturing*, *56*, 102903.

[8] Jiang, J., Xu, X., & Stringer, J. (2018). Support structures for Additive Manufacturing: A Review. *Journal of Manufacturing and Materials Processing*, *2*(4), 64.

[9] Donadello, S., Furlan, V., Demir, A. G., & Previtali, B. (2022). Interplay between powder catchment efficiency and layer height in self-stabilized laser metal deposition. *Optics and Lasers in Engineering*, *149*, 106817.

[10] Nycz, A., Lee, Y., Noakes, M., Ankit, D., Masuo, C., Simunovic, S., Bunn, J., Love, L., Oancea, V., Payzant, A., & Fancher, C. M. (2021). Effective residual stress prediction validated with neutron diffraction method for metal large-scale additive manufacturing. *Materials & Design*, *205*, 109751.

[11] Schneider, T., Hu, Y., Gao, X., Dumas, J., Zorin, D., & Panozzo, D. (2022). A large-scale comparison of tetrahedral and hexahedral elements for solving elliptic pdes with the finite element method. *ACM Transactions on Graphics*, *41*(3), 1–14.

[12] Biegler, M., Marko, A., Graf, B., & Rethmeier, M. (2018). Finite element analysis of in-situ distortion and bulging for an arbitrarily curved additive manufacturing directed energy deposition geometry. *Additive Manufacturing*, *24*, 264–272.

[13] Ansys, Inc. ANSYS (2022 R2). Available online: https://www.ansys.com.